

# Plasma Parameters from Quasi-Thermal Noise Observed by Parker Solar Probe: A New Model for the Antenna Response

Mihailo M Martinović<sup>1</sup>, Antonije Djordjevic<sup>2</sup>, Kristopher Gregory Klein<sup>1</sup>, Milan Maksimovic<sup>3</sup>, Karine Issautier<sup>4</sup>, Mingzhe Liu<sup>4</sup>, Marc Pulupa<sup>5</sup>, Stuart Bale<sup>5</sup>, Jasper S. Halekas<sup>6</sup>, and Michael McManus<sup>5</sup>

<sup>1</sup>University of Arizona

<sup>2</sup>Serbian Academy of Sciences and Arts, 11000 Belgrade, Serbia

<sup>3</sup>CNRS Délégation Ile-de-France Ouest et Nord, Paris Observatory

<sup>4</sup>LESIA

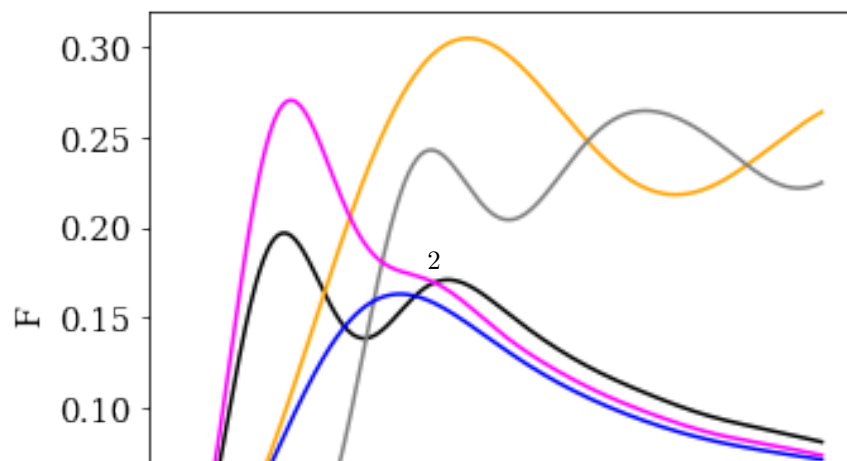
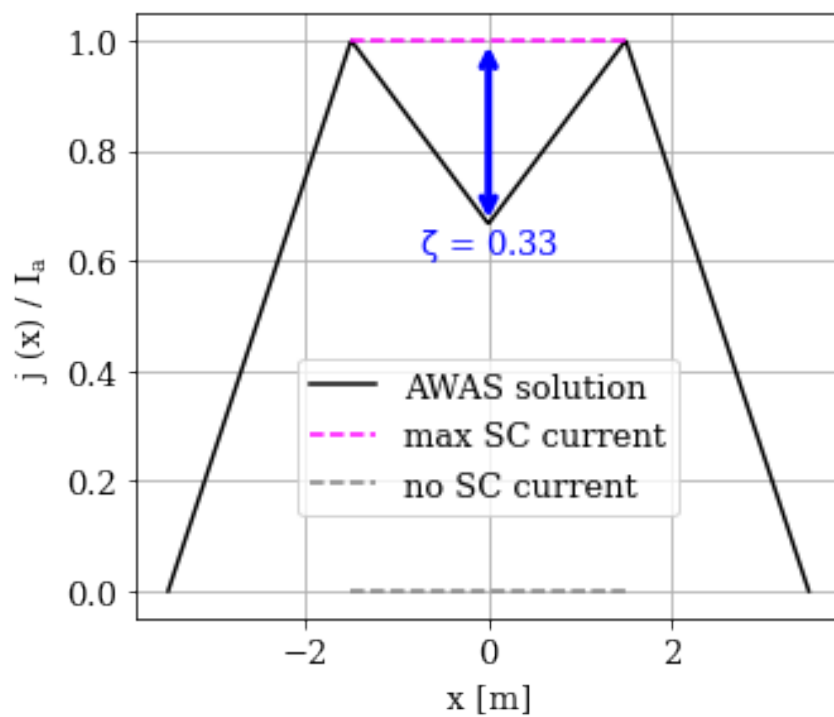
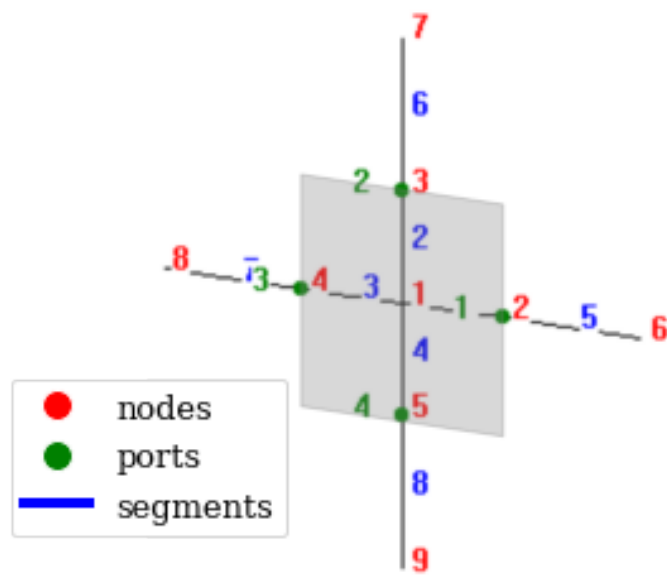
<sup>5</sup>University of California Berkeley

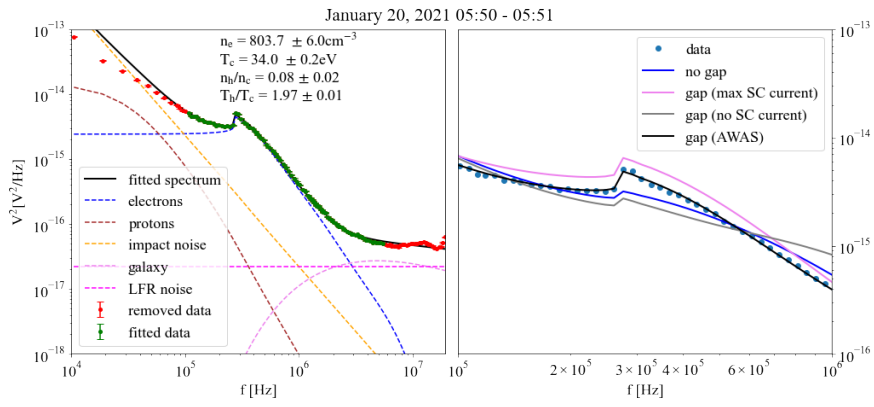
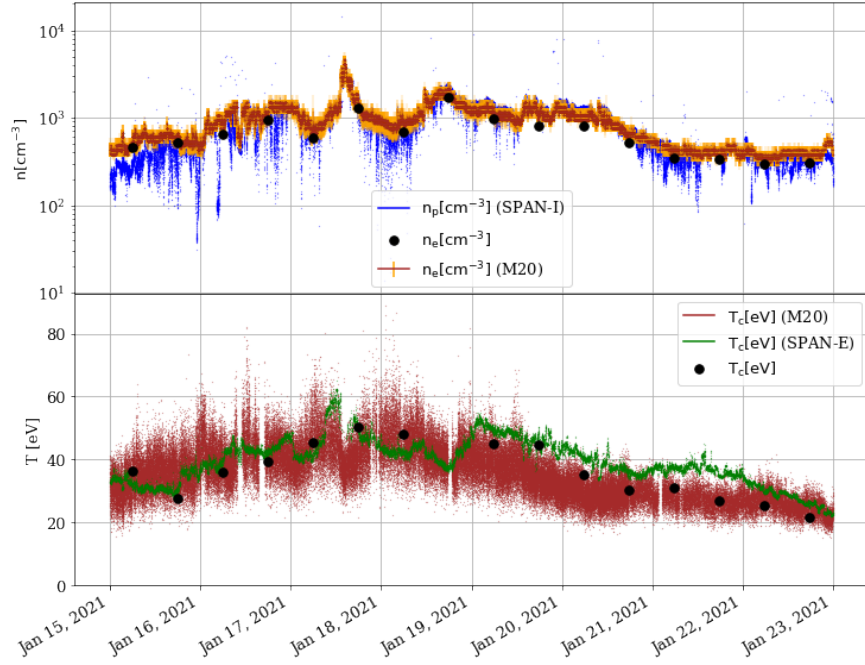
<sup>6</sup>University of Iowa

November 21, 2022

## Abstract

Quasi-Thermal Noise (QTN) spectroscopy is a reliable diagnostic routinely used for measuring electron density and temperature in space plasmas. The observed spectrum depends on both antenna geometry and plasma kinetic properties. Parker Solar Probe (PSP), launched in 2018, is equipped with an antenna system consisting of two linear dipoles with a significant gap between the antenna arms. Such a configuration, not utilized on previous missions, cannot be completely described by current models of the antenna response function. In this work, we calculate the current distribution and the corresponding response function for the PSP antenna geometry, and use these results to generate synthetic QTN spectra. Applying this model to the Encounter 7 observations from PSP provides accurate estimations of electron density and temperature, which are in very good agreement with particle analyzer measurements.





1                   **Plasma Parameters from Quasi-Thermal Noise**  
2                   **Observed by Parker Solar Probe: A New Model for the**  
3                   **Antenna Response**

4                   **Mihailo M. Martinović<sup>1,2</sup>, Antonije R. Đorđević<sup>3,4</sup>, Kristopher G. Klein<sup>1</sup>,**  
5                   **Milan Maksimović<sup>2</sup>, Karine Issautier<sup>2</sup>, Mingzhe Liu<sup>2</sup>, Marc Pulupa<sup>5</sup>, Stuart D.**  
6                   **Bale<sup>5,6,7,8</sup>, Jasper S. Halekas<sup>9</sup> and Michael D. McManus<sup>5</sup>**

7                   <sup>1</sup>Lunar and Planetary Laboratory, University of Arizona, Tucson, AZ 85721, USA.

8                   <sup>2</sup>LESIA, Observatoire de Paris, Université PSL, CNRS, Sorbonne Université, Université de Paris, 92195

9                   Meudon, France.

10                   <sup>3</sup>School of Electrical Engineering, University of Belgrade, 11000 Belgrade, Serbia

11                   <sup>4</sup>Serbian Academy of Sciences and Arts, 11000 Belgrade, Serbia

12                   <sup>5</sup>Space Sciences Laboratory, University of California, Berkeley, CA 94720-7450, USA

13                   <sup>6</sup>School of Physics and Astronomy, Queen Mary University of London, London E1 4NS, UK

14                   <sup>7</sup>Physics Department, University of California, Berkeley, CA 94720-7300, USA

15                   <sup>8</sup>The Blackett Laboratory, Imperial College London, London, SW7 2AZ, UK

16                   <sup>9</sup>Department of Physics and Astronomy, University of Iowa, IA 52242, USA

17                   **Key Points:**

- 18                   • We model the antenna response for the unique geometry of linear dipole antenna  
19                   containing a gap between arms
- 20                   • This antenna response is used to improve plasma parameters determination from  
21                   the observed quasi-thermal noise spectrum
- 22                   • The proposed model yields derived electron parameters consistent with those from  
23                   the SWEAP/SPAN instrument suite onboard Parker Solar Probe

**Abstract**

Quasi-Thermal Noise (QTN) spectroscopy is a reliable diagnostic routinely used for measuring electron density and temperature in space plasmas. The observed spectrum depends on both antenna geometry and plasma kinetic properties. Parker Solar Probe (PSP), launched in 2018, is equipped with an antenna system consisting of two linear dipoles with a significant gap between the antenna arms. Such a configuration, not utilized on previous missions, cannot be completely described by current models of the antenna response function. In this work, we calculate the current distribution and the corresponding response function for the PSP antenna geometry, and use these results to generate synthetic QTN spectra. Applying this model to the Encounter 7 observations from PSP provides accurate estimations of electron density and temperature, which are in very good agreement with particle analyzer measurements.

**Plain Language Summary**

Parker Solar Probe (PSP) is a NASA mission that is travelling much closer to the Sun than any previous spacecraft. A primary consequence of this specific trajectory are multiple adaptations in the design of instruments (radio instruments, magnetometers, particle detectors etc.) and their complex accommodations on the spacecraft. This article investigates effects of the specific PSP radio antenna geometry to high-frequency electric field observations. We apply Quasi-Thermal Noise Spectroscopy, a well established method for determining plasma density and temperature, to PSP instruments, and validate the results by comparing the parameter values from radio observations to the ones obtained by particle analyzers onboard PSP.

**1 Introduction**

QTN spectroscopy, theoretically described more than half a century ago (Andronov, 1966; Fejer & Kan, 1969), is a powerful tool to diagnose space plasmas using a passive electric antenna related to a sensitive radio receiver. Since this method was fully expanded to solar wind and pioneered aboard *ISEE-3* (Meyer-Vernet, 1979; Hoang et al., 1980), it has been routinely used to infer in-situ electron densities and temperatures on various missions in the solar wind: *IMP-6* (Kellogg, 1981), *Ulysses* (Maksimovic et al., 1995; Issautier et al., 1996, 1999; Le Chat et al., 2011), *Wind* (Maksimovic et al., 1998; Issautier et al., 2005; Martinović et al., 2020), *STEREO* (Zouganelis et al., 2010; Martinović et al., 2016), and planetary missions such as *Cassini* (Moncuquet et al., 1997, 2005).

QTN spectrum depends on two sets of inputs: 1) kinetic plasma properties, reflected through the electron VDF shape, and described by characteristic plasma functions that depend on the VDF, and 2) antenna shape and configuration, described by the antenna response function (ARF). For a comprehensive review of the QTN spectroscopy theory see e.g. Meyer-Vernet and Perche (1989); Meyer-Vernet et al. (2017). All the aforementioned missions have significantly different characteristic spectra due to different antenna configurations. These differences can be summed up in two broad categories: 1) the visibility of the plasma peak just above the electron plasma frequency  $f_p = \omega_p/2\pi = (2\pi)^{-1}\sqrt{n_e e^2/\epsilon_0 m_e}$ , depending on the ratio between the antenna length  $L_{ant}$  and Debye length  $L_D$ , where  $L_D = \sqrt{\epsilon_0 k_b T_e/n_e e^2}$  and 2) the effects of the impact noise, determined by the ratio of the antenna length to its radius  $L_{ant}/a_{ant}$ . Here,  $\epsilon_0$  is the dielectric permittivity of vacuum,  $k_b$  is the Boltzmann constant, and  $n_e$ ,  $e$  and  $m_e$  are electron density, charge and mass, respectively. A common feature of spacecraft launched before *PSP* was a dipole antenna configuration with a negligibly small gap between the antenna arms, and the spacecraft body effects being also considered as negligible. The *PSP* FIELDS suite (Bale et al., 2016) is equipped with a set of two wire dipoles, with each arm  $L_{ant} = 2\text{m}$  long. The spacecraft (SC) body separates the antenna ports, creating a gap between the arms of each dipole of  $2d = 2.98\text{m}$ , a length comparable to  $L_{ant}$ . Configurations that fea-

74 ture the gap operate only on *PSP* FIELDS (Bale et al., 2016) and *Solar Orbiter* Radio  
 75 and Plasma Waves (RPW) (Maksimović, Bale, Chust, et al., 2020) instruments, and ini-  
 76 tial observations showed that the total electron density could be inferred by locating the  
 77 peak of the signal at  $f_p \sim \sqrt{n_e}$  (Bale et al., 2019). However, the shape of the observed  
 78 QTN spectra cannot be modelled by the ARFs derived for the case of dipoles without  
 79 a gap (Kuehl, 1966, 1967). As the discrepancies due to this gap primarily appear in the  
 80 vicinity of the plasma peak, preliminary studies were able to estimate electron core tem-  
 81 perature  $T_c$  (Moncuquet et al., 2020) and total temperature  $T_e$  (Maksimović, Bale, Berčić,  
 82 et al., 2020; Liu et al., 2021) by separately analyzing power levels below and above  $f_p$ ,  
 83 respectively.

84 The primary task of this paper is to characterize the FIELDS QTN spectrum shape  
 85 given the unique instrument configuration by providing a single model valid both below  
 86 and above  $f_p$ . To accomplish this, in Section 2 we derive the ARF using the antenna and  
 87 (SC) current distribution calculated using the AWAS software (Đorđević et al., 2002).  
 88 Then, in Section 3 we calculate the theoretical model of the QTN spectrum and fit it  
 89 to observations from *PSP* Encounter 7 (E7) for periods where the antenna was unbiased.  
 90 The results show very good agreement with observations obtained by the SWEAP SPAN  
 91 instrument suite (Kasper et al., 2016; Whittlesey et al., 2020) and previous preliminary  
 92 QTN spectrum processing (Moncuquet et al., 2020). Finally, we discuss the future use  
 93 of this model, as well as potential shortcomings in Section 4.

## 94 2 Methods

### 95 2.1 FIELDS instrument observations

96 On *PSP*, the RFS component of the FIELDS suite collects the electric field fluc-  
 97 tuations up to 19.2 MHz (Pulupa et al., 2017). Within RFS, LFR and HFR cover fre-  
 98 quency ranges of 10 kHz – 1.7 MHz and 1.3 – 19.2 MHz, respectively, both with 64 log-  
 99 arithmically spaced frequencies, providing  $\sim 4.5\%$  resolution. The measurements of in-  
 100 terest for this work are collected in dipole mode, where the difference of voltages at the  
 101 antenna terminals is processed using a Polyphase Filter Bank and Fast Fourier Trans-  
 102 form algorithm. The spectra downloaded to ground at standard  $\sim 3.5s$  cadence are av-  
 103 erages of several tens of sampled spectra, where the statistical uncertainty of the power  
 104 in each averaged spectrum is held below 0.3 dB (Pulupa et al., 2017). During specified  
 105 parts of each encounter, bias current is applied to the antennas in order to keep the an-  
 106 tenna potential close to the potential of the undisturbed plasma. Applying the bias cur-  
 107 rent maximizes the response of the low frequency voltage measurement to the electric  
 108 field signals of interest, while minimizing the response to plasma density fluctuations.  
 109 Unfortunately, the biased current produces an increased impact noise signal just below  
 110 the plasma frequency. As compensating for this bias-induced signal is beyond the intended  
 111 scope of this work, we will only focus on time periods where the FIELDS antennas were  
 112 not biased. This approach was enabled during *PSP* E7, as unbiased intervals appear daily  
 113 (Jan 15-22, 2021), lasting 2 times 4 minutes for each dipole. In this work, we focus on  
 114 V1-V2 dipole, that operated with no bias during 05:48 - 05:52 and 17:48 - 17:52 each day.  
 115 In lieu of applying an algorithm that filters out low-frequency non-QTN signal compo-  
 116 nents, such as wave activity and instrument gain effects, from the spectrum (Martinović  
 117 et al., 2020), we use only the signal above 100 kHz, corresponding to approximately  $0.25f_p$ ,  
 118 avoiding the resistively coupled antenna regime (Bonnell et al., 2019). We derive the plasma  
 119 parameters from both the full resolution observations, and one minute median values,  
 120 with medians having a purpose of removing any short term signal pollution. Electron  
 121 VDF moments—core and halo density and temperature, are found via standard Levenberg-  
 122 Marquardt least square fit of merged LFR/HFR data and theoretical spectra explained  
 123 below. Proton parameters are used as errorless initial input, and are provided by fitting  
 124 the SPAN-i measured proton VDFs (see, e.g. Verniero et al. (2020)).

## 2.2 Quasi-Thermal Noise Spectroscopy

The QTN is modelled for a proton-electron plasma, with the electron VDF consisting of two isotropic Maxwellians—a thermal core and suprathermal halo, and the proton VDF being a charge-neutralizing background isotropic Maxwellian. The synthetic QTN spectrum  $V^2(f)$  is calculated using contributions from electrons  $V_{\text{qtn}}^2$ , protons  $V_{\text{pn}}^2$ , impact (shot) noise  $V_{\text{sn}}^2$  and galaxy radiation  $V_{\text{gal}}^2$  as

$$V^2 = \Gamma^2 (V_{\text{qtn}}^2 + V_{\text{pn}}^2 + V_{\text{sn}}^2 + V_{\text{gal}}^2) + V_{\text{ifr}}^2. \quad (1)$$

Here,  $\Gamma$  is the antenna gain and the instrument noise is estimated to be  $V_{\text{ifr}}^2 \approx 2.3 \cdot 10^{-17} \text{V}^2/\text{Hz}$  (Bale et al., 2016; Maksimović, Bale, Berčić, et al., 2020). Proton noise  $V_{\text{pn}}^2$ , important below  $f_p$ , is estimated assuming the solar wind velocity  $\mathbf{v}_{\text{sw}}$  is perpendicular to the FIELDS antenna, using the functional form given by Equation 22 from Issautier et al. (1999). We find proton contribution to be small compared to the impact noise at low frequencies close to perihelion, in agreement with theoretical predictions (Meyer-Vernet et al., 2017), but it still must be included for analysis close to  $f_p$ . Impact noise  $V_{\text{sn}}^2$  is calculated using Equation 15 from Martinović et al. (2016), and is very small compared to  $V_{\text{qtn}}^2$  near the peak. The level of the galaxy radiation power  $V_{\text{gal}}^2$  is calculated using the model given by Novaco and Brown (1978), with same parameters used in the Encounter 1 (E1) study by Maksimović, Bale, Berčić, et al. (2020). The galaxy and instrument noise signals are non-negligible only at very high frequency end of the spectrum and are expected to have only a minor contribution to the estimated values of halo temperature. For an isotropic Maxwellian, the electron contribution is (Chateau & Meyer-Vernet, 1989)

$$V_{\text{qtn}}^2(\omega) = \frac{16m_e\omega_p^2}{\pi\epsilon_0} \int_0^\infty \frac{B(k, \omega)F(k)}{k^2|\epsilon_L(k, \omega)|^2} dk. \quad (2)$$

Plasma VDF functions  $B(k, \omega)$  and  $\epsilon_L(k, \omega)$  describe total amount of energy of the plasma and its response to fluctuations, respectively. These two functions are determined by plasma properties only, are not affected by the instrumentation and are explained in detail elsewhere (Meyer-Vernet & Perche, 1989; Martinović, 2016). The ARF  $F(\mathbf{k})$  is given as a Fourier transform of the antenna current  $\mathbf{j}_a(\mathbf{k})$  along the dipole, normalized to a value at the antenna terminals  $I_a$ , and integrated over the entire solid angle  $\Omega$  for a given value of wavevector  $\mathbf{k}$

$$F(k) = \frac{1}{32\pi} \int \frac{|\mathbf{k} \cdot \mathbf{j}_a(\mathbf{k})|^2}{I_a^2} d\Omega \quad (3)$$

From Equation 3 it is clear that the structure of the antenna current distribution  $\mathbf{j}_a(\mathbf{r})$  significantly impacts the determination of the ARF.

## 2.3 Determination of current distribution via AWAS software

In order to characterize the antenna current distribution, we use the AWAS software package (Đorđević et al., 2002). AWAS is a versatile program for analyzing wire antennas and scatterers assembled from arbitrarily located and interconnected straight-line segments. Wire antennas can be modeled in free space, as done below, or located above a perfectly conducting plane, and can be analyzed in transmitting or receiving modes to calculate port matrix parameters, current distribution, near fields, and far fields.

The *top panel* of Figure 1 shows the 2D AWAS model of *PSP*. The SC body (shaded in grey) is approximated by a simple set of four orthogonal conductive wires, marked as segments 1-4 (blue numbers), extending between the node (reference point in the coordinate system marked by a red number) 1 and 2-5, respectively. The two dipoles are modeled as pairs of segments (5,7) and (6,8). Ports (antenna terminals) are marked by green dots and modelled as ideal current generators. Dimensions of segments reflect the FIELDS configuration, with wire segments 1-4 that replace the SC body being 1.49 m long, and antenna segments 5-8 2 m long (Bale et al., 2016). We assign the x axis to a line of a

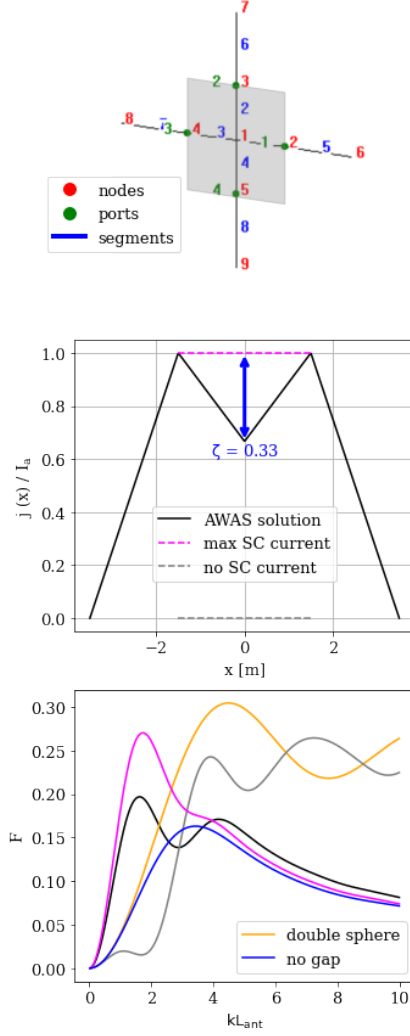


**Figure 1.** *Top:* PSP model in AWAS, with nodes (red), ports (green), and segments (blue) indicated (with labels for segment 1 and port 1 overlapped on each other). The SC body, which the model replaces with wires, is shaded in grey. *Middle:* AWAS solution for the current distribution between nodes 6 and 8 from the *top panel* (black), compared to models with the current flowing through the SC body having maximum (pink) (Meyer-Vernet & Perche, 1989) or zero value (grey). The current drops by a factor of  $\zeta \approx 1/3$  compared to the values at antenna terminals. *Bottom:* Antenna response function calculated for various antenna configurations described in the text. The color coding for the unlabeled lines is the same as on the *middle panel*.

172 linear dipole extending between nodes 6 ( $x = 3.49$  m) and 8 ( $x = -3.49$  m), where the  
 173 point of origin is at the center of the SC 2D quadratic geometry.

174 Once the antenna geometry is set, AWAS calculates currents and fields in and around  
 175 antennas by solving a two-potential equation (see, e.g. (Đorđević et al., 1979; Popović  
 176 et al., 1982)). This equation is numerically solved using the method of moments (Harrington,  
 177 1993) with the current distribution approximated by a polynomial (Đorđević et al., 1991).  
 178 This way, we provide values of the antenna current at any point within segments 1-8.  
 179 Details of the procedure are given in Chapter 6 of (Đorđević et al., 2002).

180 We model the system as a transmitting antenna in a vacuum, which corresponds  
 181 to a receiving antenna in a medium via reciprocity theorem (see, e.g. (Schelkunoff & Friis,  
 182 1952; Balanis, 1997)). The current at ports 1 and 2 is set to an arbitrary value of  $I_a =$   
 183  $1A$ , while currents at the opposite sides of the SC body for each dipole—ports 3 and 4,  
 184 respectively—are set to  $-I_a$ . Middle panel shows one-dimensional cut through the AWAS  
 185 solution along  $x$  axis with normalized values of the current. The normalized current  $j_x/I_a$   
 186 is found to be lower in intensity within segments 1 and 3, with a minimum value at  $1 -$   
 187  $\zeta \approx 2/3$  of maximum at ports 1 and 3. Therefore, the resulting profile suggests a linear  
 188 decay inside the SC body, with a minimum being different for a factor  $\zeta$  compared  
 189 to the one at the terminals. The numerical value  $\zeta \sim 0.33$  is justified *a posteriori* in  
 190 application to FIELDS data. This is notably lower than the prediction of maximum current  
 191 throughout the SC body (Meyer-Vernet & Perche, 1989), given by pink dashed line.  
 192 This current distribution will be used to calculate the antenna response, and then QTN  
 193 spectrum.

### 194 3 Results and Discussion

#### 195 3.1 Antenna response function for FIELDS

196 Assuming a current in the  $x$  direction, the Fourier transform of the current distri-  
 197 bution calculated by AWAS is given as

$$198 \quad j_x(k_x) = \frac{2(\zeta(\cos(k_x d) - 1) + k_x d \sin(k_x d))}{k_x^2 d} -$$

$$199 \quad \frac{2(k_x L_{ant} \sin(k_x d) + \cos(k_x(d + L_{ant})) - \cos(k_x d))}{k_x^2 L_{ant}} \quad (4)$$

200 This expression can be directly inserted in Equation 3. While analytical integration of  
 201 this expression is not possible, a numerical solution is given as a black line on the *bot-*  
 202 *tom panel* of Figure 1. The obtained function has similarities with both linear and spher-  
 203 ical dipole solutions, with the two peaks corresponding to the peaks of these two func-  
 204 tions. Namely, for very large wavelengths (small  $k$ ) the antenna samples waves that span  
 205 across the entire SC. In this regime, the response is dominated by the current close to  
 206 and across the SC body, having the dominant signal for the case of maximum current  
 207 through the SC body (magenta), while AWAS solution has a lower response due to non-  
 208 zero value of parameter  $\zeta$ . For smaller wavelengths (larger  $k$ ), the antenna arms increas-  
 209 ingly sample uncorrelated signals. Here, the response of a hypothetical configuration with  
 210 zero SC current (grey) starts behaving like a dipole of infinitely small spheres at distance  
 211  $2L_{ant}$  (orange), while the AWAS solution shows a slight increase in signal due to this ef-  
 212 fect before settling to a linear decrease characteristic for a linear dipole with no gap (blue).

213 We interpret this result as a consequence of the ratio  $L_{ant}/d \sim 1$ . If the antenna  
 214 arms are long compared to the gap ( $L_{ant}/d \gg 1$ ), then the gap can be neglected, re-  
 215 ducing the problem to the one encountered by multiple previous missions. Another asymp-  
 216 totic behavior is for the case  $L_{ant}/d \ll 1$ , where it reduces to a theoretical double sphere  
 217 dipole configuration. However, as neither of these approximate results was valid for *PSP*  
 218 configuration, numerical evaluation of ARF is necessary.

### 3.2 Plasma parameters from QTN spectroscopy

In this Section, we apply the new antenna response model, detailed in Section 2.3, to QTN spectra from *PSP* E7 to extract electron VDF parameters. The *left panels* of Figure 2 show examples of fits to 1-minute median values of RFS data sampled with unbiased V1-V2 dipole. Due to the very large number of sampled spectra during each of the 1-minute intervals, every panel shown represents a median of 14-17 downloaded spectra. Each spectrum downloaded from the spacecraft is an average of 40-80 on-board samples. Therefore, an instrument performs a total of 680-1360 observations per minute, and estimated uncertainty of the 1-minute averaged spectrum data points is 0.05–0.08 dB. The fitted part of the spectrum, shown as green dots, is essentially comprised of only QTN, instrument noise and galaxy radiation contributions, which allows for an accurate determination of electron VDF parameters with very small uncertainties. For each of 64 1-minute spectra (sampled for 8 days during 8 minutes per day when no antenna biasing was applied; see Section 2.1), we use multiple sets of initial guesses for electron parameters  $n_e$ ,  $T_c$ ,  $n_h/n_c$  and  $T_h/T_c$  to find absolute  $\chi^2$  minimum, and also visually inspect the fits. Then, the results from these 1-minute fits are used as an initial guess for fitting the spectra in full resolution.

On *right panels*, we compare the best fit QTN model that uses the current distribution calculated in Section 2.3 with previously applied models. As already noted above, neglecting the gap between the antenna arms (blue) does not reproduce the measured spectrum neither close to  $f_p$  nor at high frequencies. Two asymptotic SC body current models also do not produce accurate representations of the observed spectrum—if maximum uniform current is assumed (magenta), the signal is notably overestimated in the vicinity of  $f_p$ , while setting the SC current to zero in the gap region both underestimates the signal around the resonance and shows a ‘sphere dipole-like’ behavior at high frequencies, where fluctuations of larger wavelength dominantly contribute to the spectrum (Meyer-Vernet, 1979). The different shape of the illustrated curves compared to the observed spectra makes any fitting procedure unfeasible, and we were not able to obtain satisfying overall agreement with observations, or sensible values of VDF moments with any of the previously applied current distribution models. Variation of the parameter  $\zeta$  by more than  $\sim 2$ –3% also disables the model from meaningfully converging to the data, regardless of the plasma parameters used.

Figure 3 illustrates median values of fitted  $n_e$  and  $T_c$  for sets of four 1-minute unbiased intervals, plotted as black dots. We find agreement within 20% between total electron density and proton density provided by SPAN-I fits. We do not compare our results with electron density provided by SPAN-E, as it is already calibrated to  $f_p$  values obtained from the QTN plasma peak. This discrepancy is not surprising as, even though  $n_e$  is related to plasma peak frequency and is therefore the most reliable parameter in the QTN analysis, SPAN-I has a large fraction of the proton VDF moving in and out of the instrument field of view due to both instrument orientation with respect to the sunward direction (see Kasper et al. (2016); Woodham et al. (2021) for details of SPAN-I setup) and plasma flow following magnetic field reversals or ‘switchbacks’, which occur at timescales from seconds to tens of minutes (see e.g. Dudok de Wit et al. (2020); Martinović et al. (2021)). The brown line shows the values of the  $n_e$  obtained using the method introduced in Moncuquet et al. (2020) (further on referred to as M20). The M20 method relies on combination of plasma peak tracing based on the steepest slope in the QTN signal (Moncuquet et al., 2005; Kasaba et al., 2020) and fitting limited parts of the spectrum below  $f_p$  using the antenna response function given at Meyer-Vernet and Perche (1989) (violet lines at *middle* and *bottom* panels of Figure 1). Density values between the two data sets obtained from QTN observations are similar to the level of M20  $n_e$  uncertainties (orange error bars), that are of the order of  $\sim 9\%$  due to the instrument resolution. A small systematic discrepancy is notable, probably due to dependency of the plasma peak location in the frequency space from  $L_{ant}/L_D$  ratio; see Figure 2 in (Meyer-

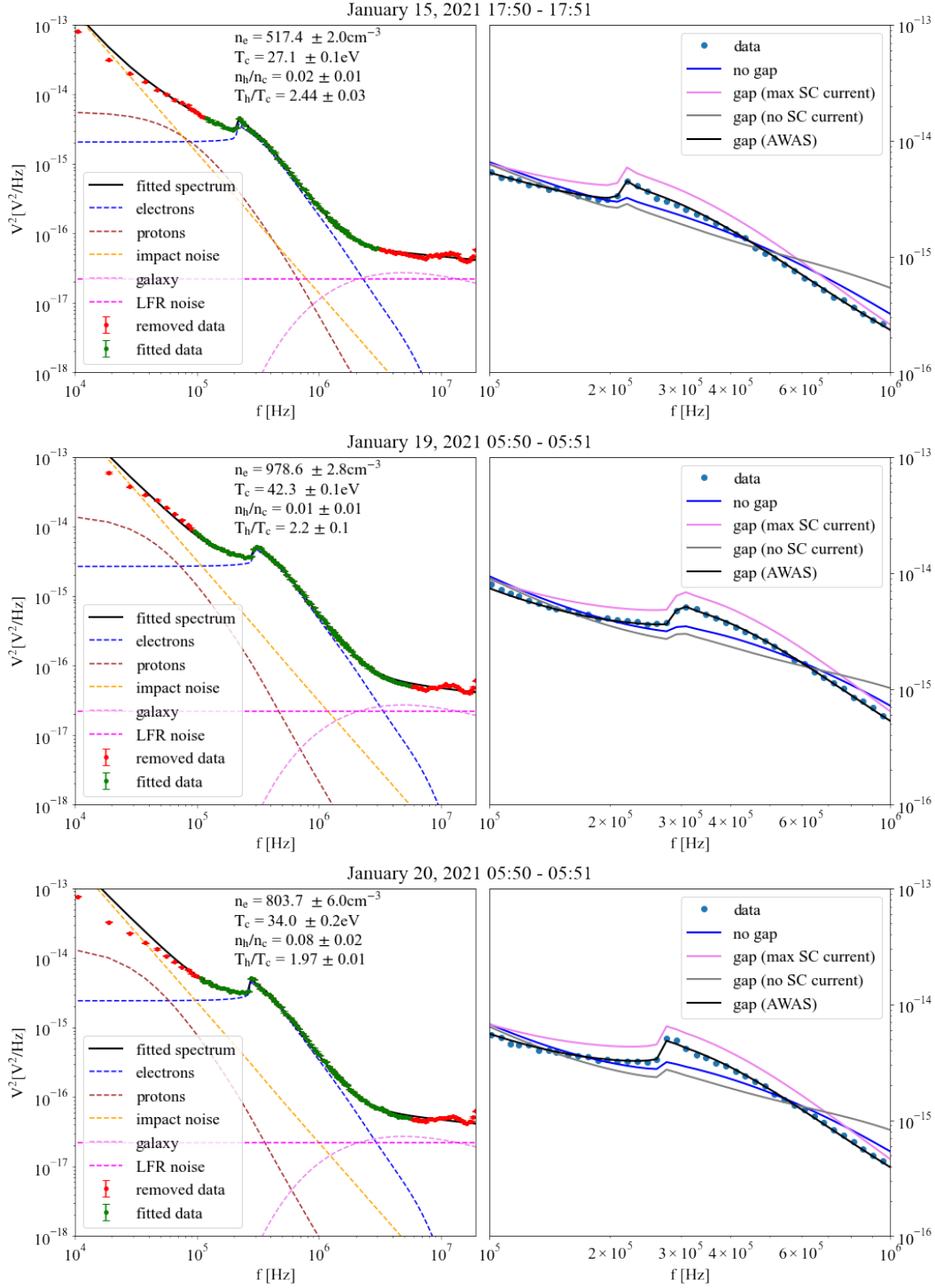


**Figure 2.** Three examples of the QTN spectrum fit. *Left:* Example of the QTN model fits to 1-minute median values of LFR V1-V2 dipole data with obtained electron parameter values and uncertainties, with  $L_{ant}/L_D \approx [1.25, 1.37, 1.38]$  from top to bottom, respectively. *Right:* Comparison of the QTN model assuming current distribution calculated via AWAS (same parameters as on the *left panels*) with other theoretical models illustrated in Figure 1, using the same color coding. Note that the double sphere dipole spectrum is an order of magnitude above the data level and is not shown.

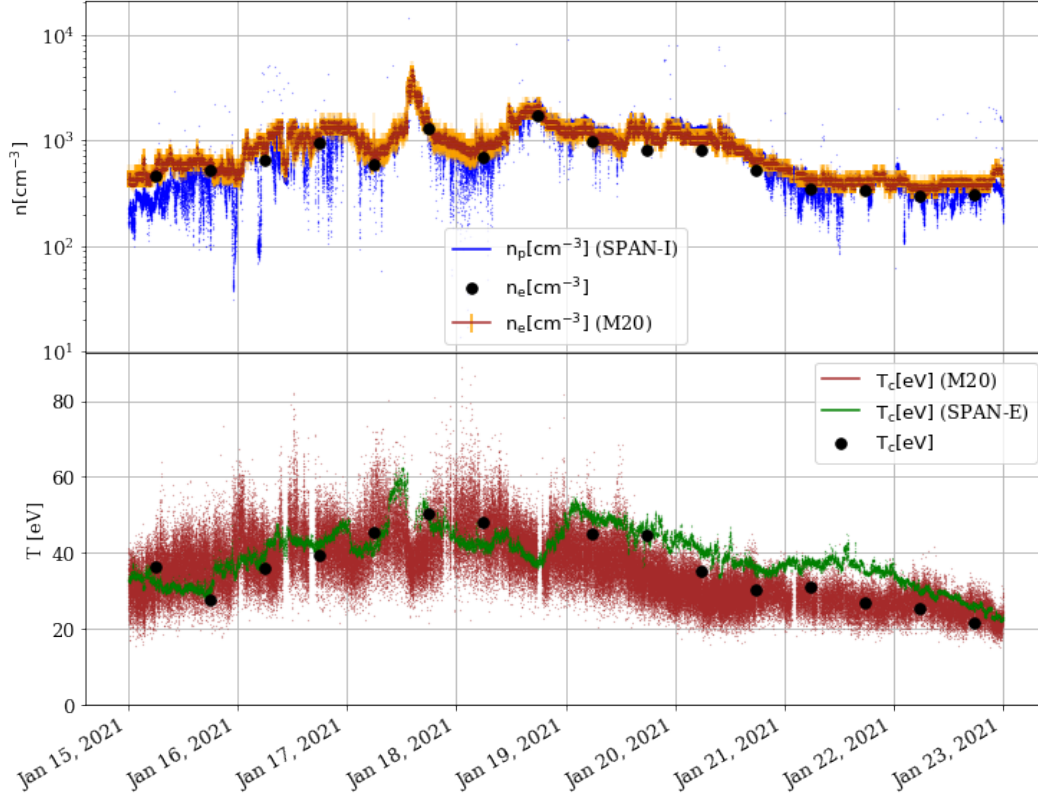


**Figure 3.** Overview of 1-minute median RFS observations fit, comparing proton (SPAN-I, blue) and electron densities from QTN spectroscopy using M20 algorithm (brown) and our model (black) on *top panel*; and electron core temperatures from SPAN-e (green) with both QTN data sets on *bottom panel*. Parameter uncertainties for black dots are of the order of the symbol size. The values of  $T_c$  from SPAN-E and our method do not differ for more than 10% for higher, and no more than 25% for lower temperatures. The missing interval in the afternoon of January 18 had a clearly resolved plasma peak, but also a significantly increased non-QTN signal below  $f_p$ , and confident estimation of  $T_c$  was not possible.

272 Vernet & Perche, 1989) for more details. These small corrections will be discussed in length  
 273 in the future when a more robust data sets become available from both later Encoun-  
 274 ters and biased intervals.

275 Values of  $T_c$  are in overall agreement with SPAN-E results, with discrepancies within  
 276 10% closer to the *PSP* E7 closest approach, increasing to  $\sim 25\%$  outbound. The differ-  
 277 ence between the two sets of results is reasonably small and we consider that its vari-  
 278 ation may be due to the change in contribution of the electron noise to the overall QTN  
 279 spectrum. First, as electron temperature increases, the error in  $V_{pn}^2$  estimate due to the  
 280 antenna orientation (Issautier et al., 1999) becomes less significant. Second, the impor-  
 281 tance of the impact noise decreases below  $f_p$  as  $T_c$  increases and the  $L_{ant}/L_D$  ratio in-  
 282 crease. The increase in discrepancy matches with the decrease of  $L_{ant}/L_D$  from  $\sim 1.4$ –  
 283  $1.5$  to  $\sim 1$  during the last three days of the observed interval. Also, precision of the SPAN-  
 284 E parameters is increased with the VDF moments due to increased signal-to-noise ra-  
 285 tio. Our results show a very good agreement in terms of general trend with  $T_c$  values pro-  
 286 vided by M20, and fall within the range of large variations. As already noted for den-  
 287 sity, a thorough discussion on the differences between the different techniques will re-  
 288 quire future analysis of unbiased intervals and is not within the scope of this paper.

289 Figure 4 shows the fitted values obtained from full resolution measurements, which  
 290 do not notably deviate from initial 1-minute fits. Standard deviations are less than 3%  
 291 for  $n_e$  (approximately half of the instrument resolution) and less than 15% for  $T_c$ . These  
 292 results demonstrate the potential for the usage of full resolution *PSP* QTN measurements  
 293 to accurately extract electron VDF parameters in the near-Sun environment, as well as  
 294 for advanced data products, such as level of the density fluctuations at sub-ion scales.  
 295 For unbiased intervals, M20 values of  $T_c$  are not provided, while values of  $n_e$  are not shown  
 296 due to very large uncertainties, which make direct comparison inconvenient.

## 297 4 Conclusions

298 QTN spectroscopy is a powerful in situ tool to accurately yield electron plasma pa-  
 299 rameters from levels of electric field fluctuations measured by an antenna in a plasma.  
 300 The unique configuration of the *PSP*/FIELDs antennas caused previously applied an-  
 301 tenna response models to either under- or overestimate the theoretical predictions around  
 302 electron plasma frequency, and therefore made fitting of the full frequency range of QTN  
 303 spectra unfeasible. In this article, we propose a new model of for the antenna response  
 304 that using a SC current distribution calculated via simplified *PSP* geometry scheme in  
 305 AWAS software. Fitting of the generic QTN model to observations provides accurate val-  
 306 ues of electron VDF parameters, with very low uncertainties and small spreads over minutes-  
 307 long time intervals.

308 Here, we must note that a more realistic description of the suprathermal electron  
 309 VDF as measured by *PSP* would include a significant strahl population, (Halekas et al.,  
 310 2020). A detailed description of how strahl electrons affect QTN spectra is an open ques-  
 311 tion and is a matter of future research. Therefore, even though our examples are in agree-  
 312 ment with recently measured strahl temperatures being  $\sim 100$  eV (Berčić et al., 2020),  
 313 initial scarce calculations show that the peak width, and therefore  $n_h$ , might be primar-  
 314 ily affected by the strahl, and the results for suprathermal parameters from this model  
 315 should be handled with care.

316 The results shown here are intended to enable future studies, primarily by expand-  
 317 ing this model to account for biased antenna signals, providing a full survey of VDF mo-  
 318 ments throughout multiple *PSP* encounters. In the theoretical realm, the primary re-  
 319 maining open question is the effect of the strahl population, which is expected to be largely  
 320 increased as we approach the Sun (Maksimović, Zouganelis, et al., 2005; Štverak et al.,  
 321 2009; Berčić et al., 2020), on the QTN spectrum. The effects of strahl are expected to

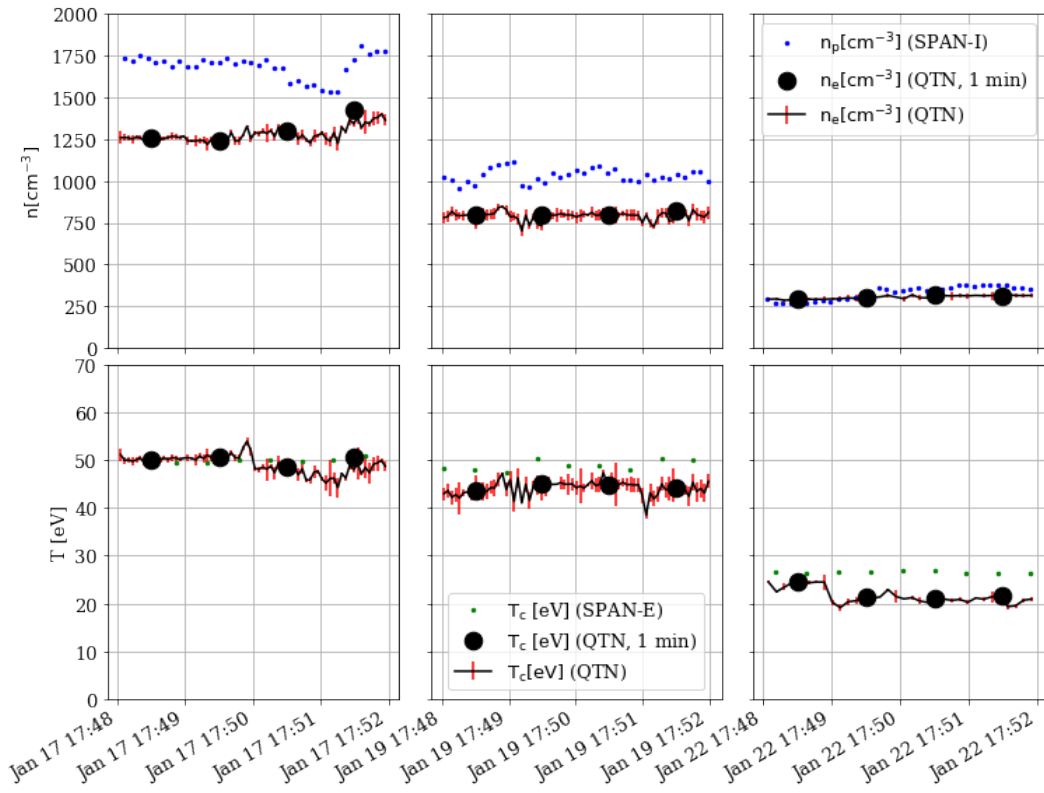


**Figure 4.** Comparison of SPAN parameters (same spatial and color scheme as on Figure 3) for three example intervals from E7 not represented on Figure 2. The full resolution fits are shown with error bars. The spread of  $T_c$  values obtained by QTN spectroscopy is lower than 20% for all 1-minute intervals.

322 be important around  $f_p$ . As mentioned above, visibility of the plasma peak, and there-  
 323 fore the strahl signal, depends on the  $L_{ant}/L_D$  ratio, which is steadily increasing as we  
 324 approach the Sun (Maksimović, Issautier, et al., 2005) and has surpassed unity during  
 325 the closest approach of *PSP* in E7. As future encounters in 2023 and 2024 are expected  
 326 to make *PSP* the first non-spinning SC with  $L_{ant}/L_D \gg 1$ , there is a potential for plasma  
 327 resonance peak to be sufficiently well resolved for small differences between halo and strahl  
 328 signals to be tested by observations.

## 329 Acronyms

330 **PSP** Parker Solar Probe  
 331 **QTN** Quasi-Thermal Noise  
 332 **VDF** Velocity Distribution Function  
 333 **STEREO** Solar TERrestrial REsearch Observatory  
 334 **AWAS** Analysis of Wire Antennas and Scatterers  
 335 **SWEAP** Solar Wind Electrons, Protons & Alphas  
 336 **SPAN-I(E)** Solar Probe ANalyzer for Ions (Electrons)  
 337 **RFS** Radio Frequency Spectrometer  
 338 **LFR** Low Frequency Receiver  
 339 **HFR** High Frequency Receiver  
 340 **SPDF** Space Physics Data Facility

## 341 Acknowledgments

342 We thank Michel Moncuquet for enlightening discussions on the LFR data processing.  
 343 Parker Solar Probe was designed, built, and is now operated by the Johns Hopkins Ap-  
 344 plied Physics Laboratory as part of NASA’s Living with a Star (LWS) program (con-  
 345 tract NNN06AA01C). Support from the LWS management and technical team has played  
 346 a critical role in the success of the Parker Solar Probe mission. The authors acknowl-  
 347 edge CNES (Centre National d Etudes Spatiales), CNRS (Centre National de la Recherche  
 348 Scientifique), the Observatoire de PARIS, NASA and the FIELDS/RFS team for their  
 349 support to the PSP/SQTN data production, and the CDPP (Centre de Donnees de la  
 350 Physique des Plasmas) for their archiving and provision. The FIELDS experiment was  
 351 developed and is operated under NASA contract NNN06AA01C. The SWEAP Inves-  
 352 tigation and this publication are supported by the PSP mission under NASA contract  
 353 NNN06AA01C. M. M. Martinović and K. G. Klein were financially supported by NASA  
 354 grant 80NSSC19K0521. PSP FIELDS LFR/HFR data is available at [http://sprg.ssl.berkeley.edu/data/psp/data/sci/fields/l2/rfs\\_lfr/](http://sprg.ssl.berkeley.edu/data/psp/data/sci/fields/l2/rfs_lfr/) and [http://sprg.ssl.berkeley.edu/data/psp/data/sci/fields/l2/rfs\\_hfr/](http://sprg.ssl.berkeley.edu/data/psp/data/sci/fields/l2/rfs_hfr/). PSP SWEAP SPAN-I/SPAN-E data can be found at <http://sweap.cfa.harvard.edu/pub/data/sci/sweap/spi/L3/> and <http://sweap.cfa.harvard.edu/pub/data/sci/sweap/spe/L3/>. The M20 data set is accessible at French national data centre for natural plasmas of the solar system <http://www.cdpp.eu/> under Missions@Archive / PARKER SOLAR PROBE MISSION / PARKER SOLAR PROBE FIELDS Experiment / PARKER SOLAR PROBE FIELDS - Simplified Quasi-Thermal Noise (SQTN) Spectroscopy.

## 363 References

364 Andronov, A. A. (1966). Импеданс и шумы антенны (зонда) в космической плаз-  
 365 мы. *Космические исследования*, 4, 558–567.  
 366 Balanis, C. A. (1997). *Antenna theory and analysis and design*. New York, USA:  
 367 Wiley.  
 368 Bale, S. D., Badman, S. T., Bonnell, J. W., Bowen, T. A., Burgess, D., Case, A. W.,

- 369 ... Wygant, J. R. (2019, December). Highly structured slow solar wind  
 370 emerging from an equatorial coronal hole. *Nature*, *576*(7786), 237-242. doi:  
 371 10.1038/s41586-019-1818-7
- 372 Bale, S. D., Goetz, K., Harvey, P. R., Turin, P., Bonnell, J. W., Dudok de Wit, T.,  
 373 ... Wygant, J. R. (2016, December). The FIELDS Instrument Suite for Solar  
 374 Probe Plus. Measuring the Coronal Plasma and Magnetic Field, Plasma Waves  
 375 and Turbulence, and Radio Signatures of Solar Transients. *Space Science*  
 376 *Reviews*, *204*(1-4), 49-82. doi: 10.1007/s11214-016-0244-5
- 377 Berčić, L., Larson, D., Whittlesey, P., Maksimović, M., Badman, S. T., Landi, S.,  
 378 ... Stevens, M. L. (2020, April). Coronal Electron Temperature Inferred  
 379 from the Strahl Electrons in the Inner Heliosphere: Parker Solar Probe  
 380 and Helios Observations. *The Astrophysical Journal*, *892*(2), 88. doi:  
 381 10.3847/1538-4357/ab7b7a
- 382 Bonnell, J. W., Mozer, F., Bale, S. D., Case, A. W., Goodrich, K., Harvey, P., ...  
 383 Wygant, J. R. (2019, December). In-Flight DC and Low-Frequency Electric  
 384 Field Calibration for the Parker Solar Probe. In *Agu fall meeting abstracts*  
 385 (Vol. 2019, p. SH13C-3439).
- 386 Chateau, Y. F., & Meyer-Vernet, N. (1989). Electrostatic noise in non-maxwellian  
 387 plasmas: Flat-top distribution function. *Journal of Geophysical Research*, *94*,  
 388 15407–15414.
- 389 Dorđević, A. R., Baždar, M. B., Petrović, V. V., Olcan, D. I., Sarkar, T. K., &  
 390 Harrington, R. F. (2002). *Awacs for windows version 2.0: Analysis of wire an-*  
 391 *tennas and scatterers (software and user's manual)*. 685 Canton St, Norwood,  
 392 MA 02062, USA: Artech House.
- 393 Dorđević, A. R., Baždar, M. B., Sarkar, T. K., & Harrington, R. F. (1991). Solution  
 394 of two-potential equation for wire structures using polynomial expansion and  
 395 pulse testing functions. In *1991 seventh international conference on antennas*  
 396 *and propagation, icap 91 (iee)* (pp. 540–543).
- 397 Dorđević, A. R., Popović, B. D., & Dragović, M. B. (1979). A method for rapid  
 398 analysis of wire-antenna structures. *Archiv für Elektrotechnik*, *61*(1), 17–23.
- 399 Dudok de Wit, T., Krasnoselskikh, V. V., Bale, S. D., Bonnell, J. W., Bowen, T. A.,  
 400 Chen, C. H. K., ... Whittlesey, P. L. (2020, February). Switchbacks in  
 401 the Near-Sun Magnetic Field: Long Memory and Impact on the Turbulence  
 402 Cascade. *The Astrophysical Journal Supplement Series*, *246*(2), 39. doi:  
 403 10.3847/1538-4365/ab5853
- 404 Fejer, J. A., & Kan, J. R. (1969). Noise spectrum received by an antenna in a  
 405 plasma. *Radio Science*, *4*, 721–728.
- 406 Halekas, J. S., Whittlesey, P., Larson, D. E., McGinnis, D., Maksimovic, M.,  
 407 Berthomier, M., ... Harvey, P. R. (2020, February). Electrons in the Young  
 408 Solar Wind: First Results from the Parker Solar Probe. *The Astrophysical*  
 409 *Journal Supplement Series*, *246*(2), 22. doi: 10.3847/1538-4365/ab4cec
- 410 Harrington, R. F. (1993). *Field computation by moment methods*. Wiley-IEEE  
 411 Press.
- 412 Hoang, S., Steinberg, J. L., Epstein, G., Tilloles, P., Fainberg, J., & Stone, R. G.  
 413 (1980). The low-frequency continuum as observed in the solar wind from isee 3  
 414 - thermal electrostatic noise. *Journal of Geophysical Research*, *85*, 3419–3430.
- 415 Issautier, K., Meyer-Vernet, N., Moncuquet, M., & Hoang, S. (1996). A novel  
 416 method to measure the solar wind speed. *Geophysical Research Letters*, *23*,  
 417 1649–1652.
- 418 Issautier, K., Meyer-Vernet, N., Moncuquet, M., & Hoang, S. (1999). Quasi-thermal  
 419 noise in a drifting plasma: Theory and application to solar wind diagnostic on  
 420 ulysses. *Journal of Geophysical Research*, *104*, 6691–6704.
- 421 Issautier, K., Perche, C., Hoang, S., Maksimović, M., Lacombe, C., Bougeret, J.-  
 422 L. H., & Salem, C. (2005). Solar wind electron density and temperature  
 over solar cycle 23: Thermal noise measurements on wind. *Advances in Space*

- 424 *Research*, *35*, 2141–2146.
- 425 Kasaba, Y., Kojima, H., Moncuquet, M., Wahlund, J.-E., Yagitani, S., Sahraoui,  
426 F., ... Usui, H. (2020, June). Plasma Wave Investigation (PWI) Aboard  
427 BepiColombo Mio on the Trip to the First Measurement of Electric Fields,  
428 Electromagnetic Waves, and Radio Waves Around Mercury. *Space Science  
429 Reviews*, *216*(4), 65. doi: 10.1007/s11214-020-00692-9
- 430 Kasper, J. C., Abiad, R., Austin, G., Balat-Pichelin, M., Bale, S. D., Belcher, J. W.,  
431 ... Zank, G. (2016, December). Solar Wind Electrons Alphas and Protons  
432 (SWEAP) Investigation: Design of the Solar Wind and Coronal Plasma Instru-  
433 ment Suite for Solar Probe Plus. *Space Science Reviews*, *204*(1-4), 131-186.  
434 doi: 10.1007/s11214-015-0206-3
- 435 Kellogg, P. (1981). Calculation and observation of thermal electrostatic noise in so-  
436 lar wind plasma. *Plasma Physics*, *23*, 735–751.
- 437 Kuehl, H. H. (1966). Resistance of a short antenna in a warm plasma. *Radio Sci-  
438 ence*, *1*, 971–976.
- 439 Kuehl, H. H. (1967). Computations of the resistance of a short antenna in a warm  
440 plasma. *Radio Science*, *2*, 73–76.
- 441 Le Chat, G., Issautier, K., Meyer-Vernet, N., & Hoang, S. (2011). Large-scale vari-  
442 ation of solar wind electron properties from quasi-thermal noise spectroscopy:  
443 Ulysses measurements. *Solar Physics*, *271*, 141–148.
- 444 Liu, M., Issautier, K., Meyer-Vernet, N., Moncuquet, M., Maksimovic, M., Halekas,  
445 J. S., ... Stevens, M. L. (2021, June). Solar wind energy flux observations  
446 in the inner heliosphere: first results from Parker Solar Probe. *Astronomy &  
447 Astrophysics*, *650*, A14. doi: 10.1051/0004-6361/202039615
- 448 Maksimović, M., Bale, S. D., Berčić, L., Bonnell, J. W., Case, A. W., Wit, T. D. d.,  
449 ... Whittlesey, P. L. (2020, February). Anticorrelation between the Bulk  
450 Speed and the Electron Temperature in the Pristine Solar Wind: First Results  
451 from the Parker Solar Probe and Comparison with Helios. *The Astrophysical  
452 Journal Supplement Series*, *246*(2), 62. doi: 10.3847/1538-4365/ab61fc
- 453 Maksimović, M., Bale, S. D., Chust, T., Khotyaintsev, Y., Krasnoselskikh, V., Kret-  
454 zschmar, M., ... Zouganelis, I. (2020, October). The Solar Orbiter Radio and  
455 Plasma Waves (RPW) instrument. *Astronomy & Astrophysics*, *642*, A12. doi:  
456 10.1051/0004-6361/201936214
- 457 Maksimovic, M., Bougeret, J. L., Perche, C., Steinberg, J. T., Lazarus, A. J., Viñas,  
458 A. F., & Fitzenreiter, R. J. (1998). Solar wind density intercomparisons on  
459 the wind spacecraft using waves and swe experiments. *Geophysical Research  
460 Letters*, *25*, 1265–1268.
- 461 Maksimovic, M., Hoang, S., Meyer-Vernet, N., Moncuquet, M., Bougeret, J. L.,  
462 Phillips, J. L., & Canu, P. (1995, Oct). Solar wind electron parameters from  
463 quasi-thermal noise spectroscopy and comparison with other measurements  
464 on Ulysses. *Journal of Geophysical Research*, *100*(A10), 19881-19892. doi:  
465 10.1029/95JA01550
- 466 Maksimović, M., Issautier, K., Meyer-Vernet, N., Perche, C., Moncuquet, M.,  
467 Zouganelis, Y., ... Bougeret, J. L. (2005). Solar wind electron tempera-  
468 ture and density measurements on the solar orbiter with thermal noise spec-  
469 troscopy. *Advances in Space Research*, *35*, 1471–1473.
- 470 Maksimović, M., Zouganelis, Y., Chaufray, J. Y., Issautier, K., Scime, E. E., Little-  
471 ton, J. E., ... Elliot, H. (2005). Radial evolution of the electron distribution  
472 functions in the fast solar wind between 0.3 and 1.5 au. *Journal of Geophysical  
473 Research*, *110*, A09104.
- 474 Martinović, M. M. (2016). *A study of quasi-thermal noise and shot noise in space  
475 plasmas* (Unpublished doctoral dissertation). LESIA, Observatoire de Paris /  
476 University of Belgrade.
- 477 Martinović, M. M., Klein, K. G., Gramze, S. R., Jain, H., Maksimović, M., Za-  
478 slavsky, A., ... Simić, Z. (2020, August). Solar Wind Electron Parame-

- 479       ters Determination on Wind Spacecraft Using Quasi-Thermal Noise Spec-  
480       troscopy. *Journal of Geophysical Research (Space Physics)*, 125(8), e28113.  
481       doi: 10.1029/2020JA028113
- 482       Martinović, M. M., Klein, K. G., Huang, J., Chandran, B. D. G., Kasper, J. C.,  
483       Lichko, E., . . . Bale, S. D. (2021, May). Multiscale Solar Wind Turbulence  
484       Properties inside and near Switchbacks Measured by the Parker Solar Probe.  
485       *The Astrophysical Journal*, 912(1), 28. doi: 10.3847/1538-4357/abebe5
- 486       Martinović, M. M., Zaslavsky, A., Maksimović, M., Meyer-Vernet, N., Šegan, S.,  
487       Zouganelis, Y., . . . Bale, S. D. (2016). Quasi-thermal noise measurements on  
488       stereo: Kinetic temperature deduction using electron shot noise model. *Journal*  
489       *of Geophysical Research: Space Physics*, 121, 129–139.
- 490       Meyer-Vernet, N. (1979). On natural noises detected by antennas in plasmas. *Jour-*  
491       *nal of Geophysical Research*, 94, 2405–2415.
- 492       Meyer-Vernet, N., Issautier, K., & Moncuquet, M. (2017). Quasi-thermal noise spec-  
493       troscopy: The art and the practice. *Journal of Geophysical Research: Space*  
494       *Physics*, 122, 7925–7945.
- 495       Meyer-Vernet, N., & Perche, C. (1989). Tool kit for antennae and thermal noise near  
496       the plasma frequency. *Journal of Geophysical Research*, 94, 2405–2415.
- 497       Moncuquet, M., Lecacheux, A., Meyer-Vernet, N., Cecconi, B., & Kurth, W. S.  
498       (2005). Quasi thermal noise spectroscopy in the inner magnetosphere of saturn  
499       with cassini/rpws: Electron temperatures and density. *Geophysical Research*  
500       *Letters*, 32, L20S02.
- 501       Moncuquet, M., Meyer-Vernet, N., Issautier, K., Pulupa, M., Bonnell, J. W., Bale,  
502       S. D., . . . Malaspina, D. M. (2020, Feb). First In Situ Measurements of Elec-  
503       tron Density and Temperature from Quasi-thermal Noise Spectroscopy with  
504       Parker Solar Probe/FIELDS. *The Astrophysical Journal Supplement Series*,  
505       246(2), 44. doi: 10.3847/1538-4365/ab5a84
- 506       Moncuquet, M., Meyer-Vernet, N., & Hoang, S. (1997). Detection of bernstein  
507       wave forbidden bands in the jovian magnetosphere: A new way to measure the  
508       electron density. *Journal of Geophysical Research*, 102, 21697–21708.
- 509       Novaco, J. C., & Brown, L. W. (1978, Apr). Nonthermal galactic emission below 10  
510       megahertz. *The Astrophysical Journal*, 221, 114-123. doi: 10.1086/156009
- 511       Popović, B. D., Dragović, M. B., & Đorđević, A. R. (1982). *Analysis and synthesis*  
512       *of wire antennas*. Chichester, UK: John Wiley & Sons.
- 513       Pulupa, M., Bale, S. D., Bonnell, J. W., Bowen, T. A., Carruth, N., Goetz, K., . . .  
514       Sundkvist, D. (2017, March). The Solar Probe Plus Radio Frequency Spec-  
515       trometer: Measurement requirements, analog design, and digital signal process-  
516       ing. *Journal of Geophysical Research (Space Physics)*, 122(3), 2836-2854. doi:  
517       10.1002/2016JA023345
- 518       Schelkunoff, S. A., & Friis, H. T. (1952). *Antennas: theory and practice*. 111 River  
519       Street, Hoboken, New York 07030, USA: Wiley.
- 520       Verniero, J. L., Larson, D. E., Livi, R., Rahmati, A., McManus, M. D., Pyakurel,  
521       P. S., . . . de Wit, T. D. (2020, May). Parker Solar Probe Observations of  
522       Proton Beams Simultaneous with Ion-scale Waves. *The Astrophysical Journal*  
523       *Supplement Series*, 248(1), 5. doi: 10.3847/1538-4365/ab86af
- 524       Whittlesey, P. L., Larson, D. E., Kasper, J. C., Halekas, J., Abatcha, M., Abiad, R.,  
525       . . . Verniero, J. L. (2020, February). The Solar Probe ANalyzers—Electrons  
526       on the Parker Solar Probe. *The Astrophysical Journal Supplement Series*,  
527       246(2), 74. doi: 10.3847/1538-4365/ab7370
- 528       Woodham, L. D., Horbury, T. S., Matteini, L., Woolley, T., Laker, R., Bale, S. D.,  
529       . . . Pulupa, M. P. (2021, June). Enhanced proton parallel temperature inside  
530       patches of switchbacks in the inner heliosphere. *Astronomy and Astrophysics*,  
531       650, L1. doi: 10.1051/0004-6361/202039415
- 532       Zouganelis, Y., Maksimović, M., Meyer-Vernet, N., Bale, S. D., Eastwood, J. P.,  
533       Zaslavsky, A., . . . Kaiser, M. L. (2010). Measurements of stray antenna

534 capacitance in the stereo/waves instrument: Comparison of the measured volt-  
535 age spectrum with an antenna electron shot noise model. *Radio science*, *45*,  
536 1005–1009.

537 Štverak, S., Maksimović, M., Travníček, P., Marsch, E., Fazakerley, A. N., & Scime,  
538 E. E. (2009). Radial evolution of nonthermal electron populations in the  
539 low-latitude solar wind: Helios, cluster, and ulysses observations. *Journal of*  
540 *Geophysical Research*, *114*, A05104.

Figure 1.

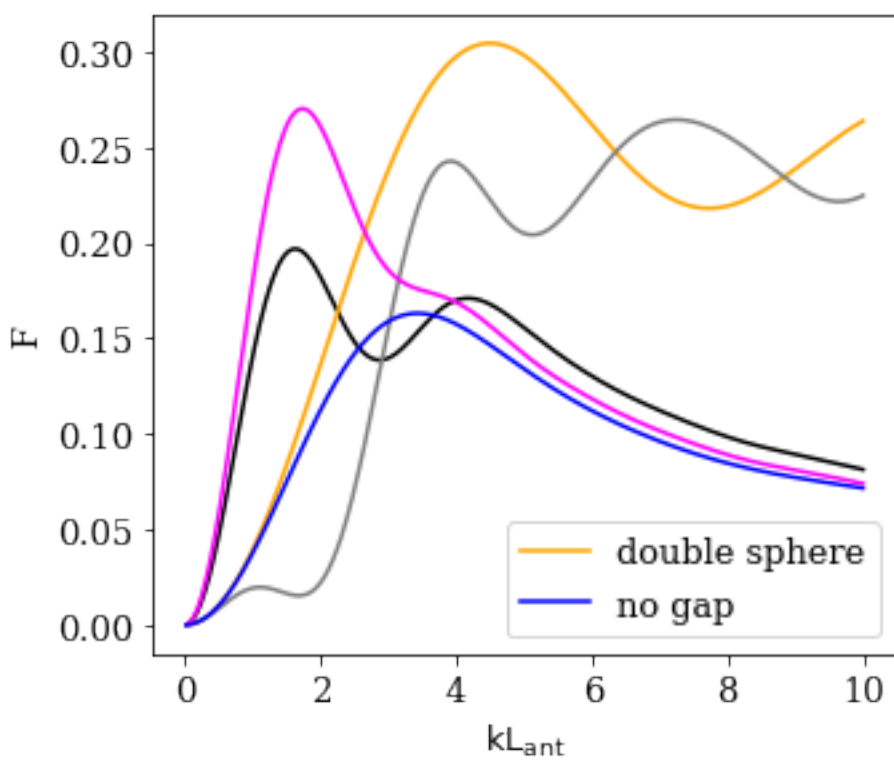
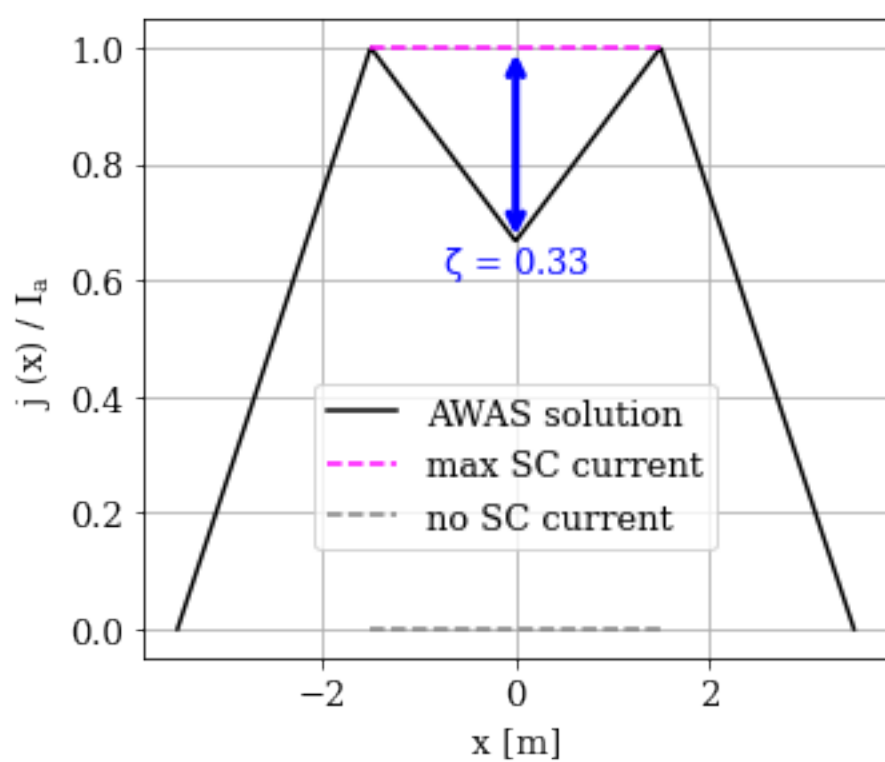
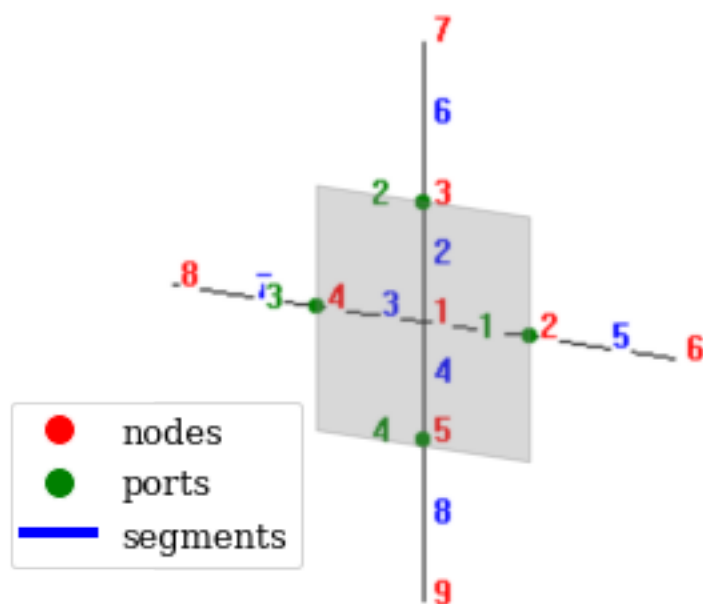


Figure 2\_1.

January 15, 2021 17:50 - 17:51

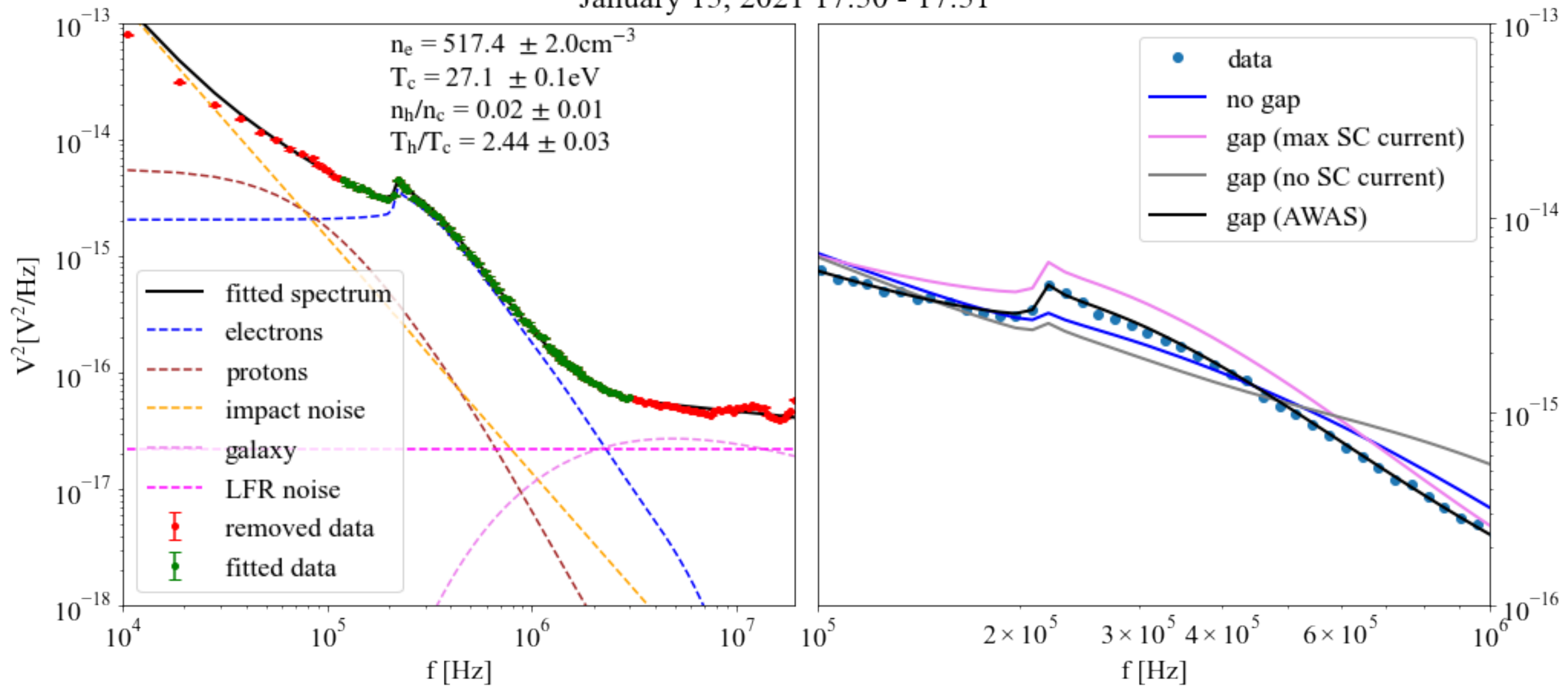


Figure 2\_2.

January 19, 2021 05:50 - 05:51

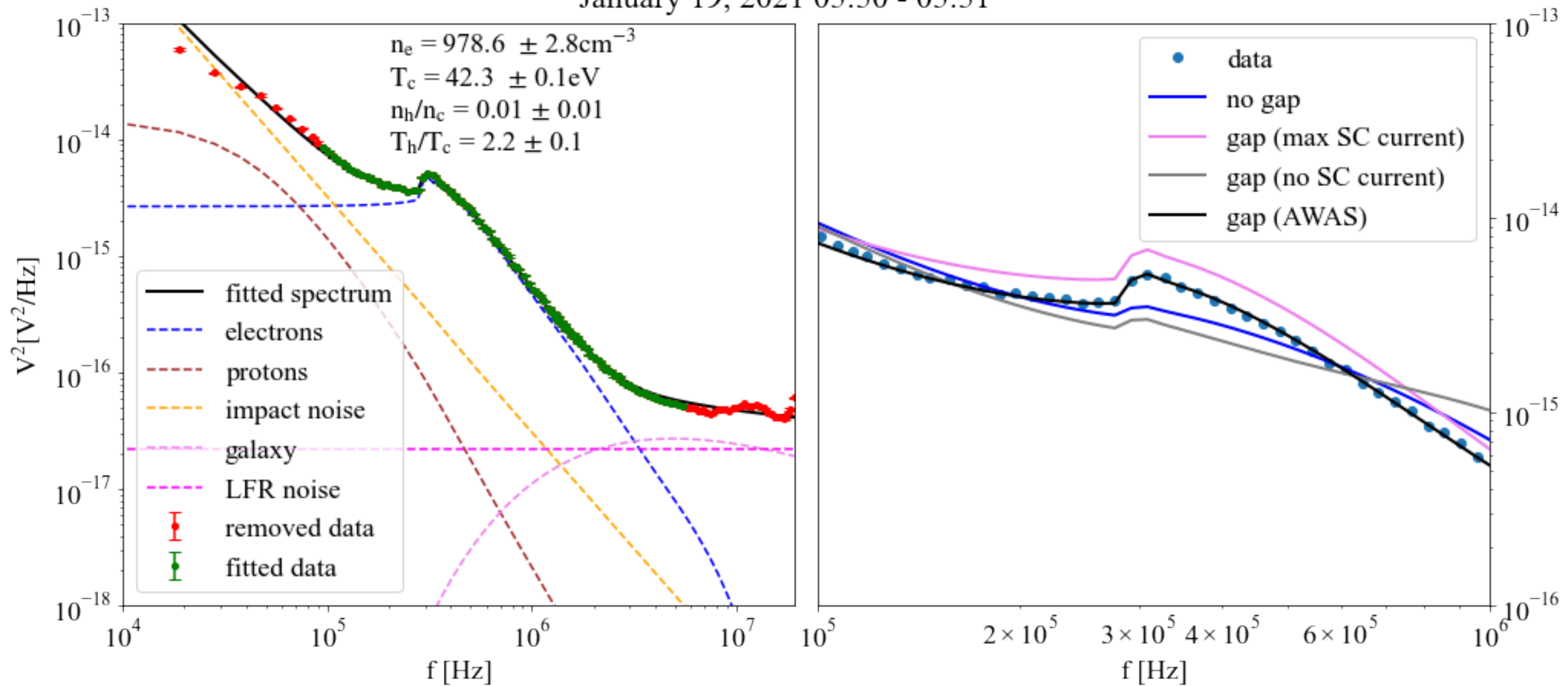


Figure 2\_3.

January 20, 2021 05:50 - 05:51

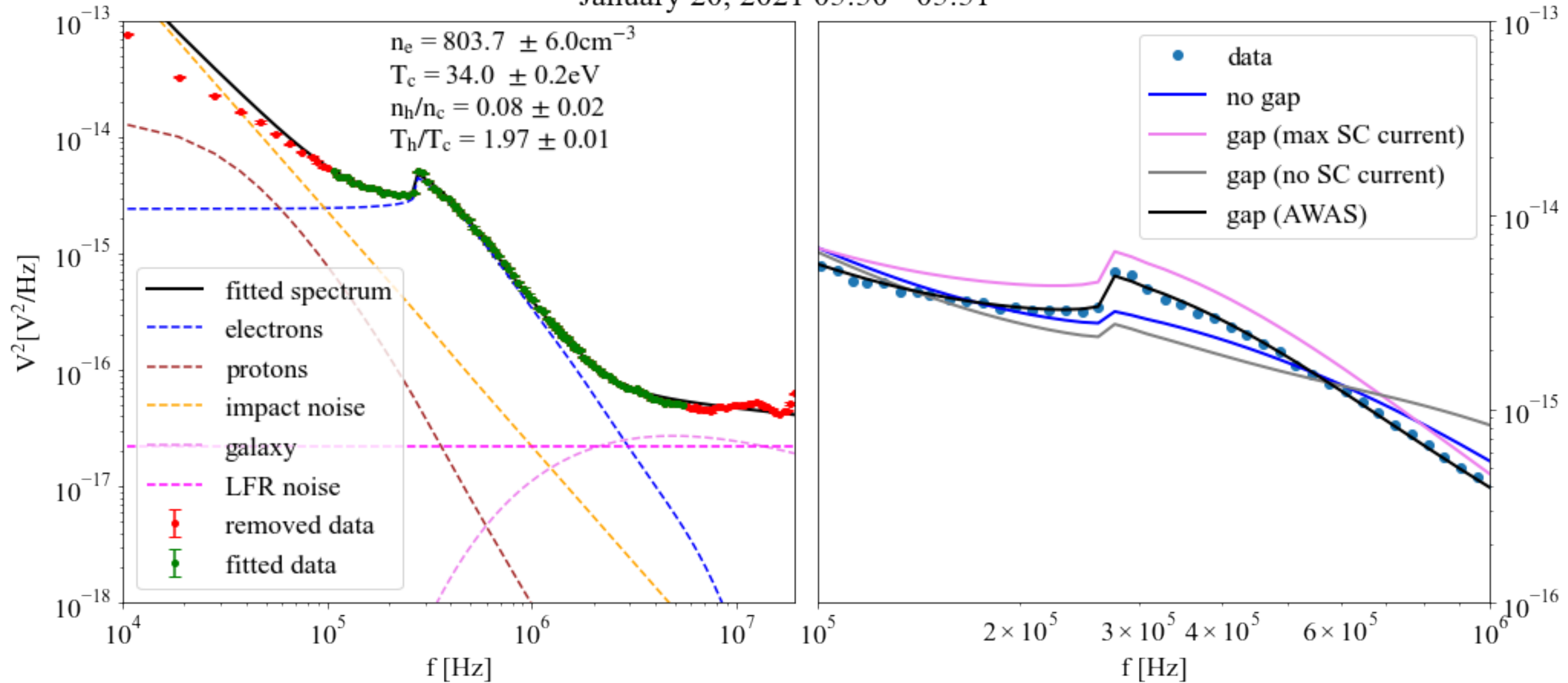


Figure 3.

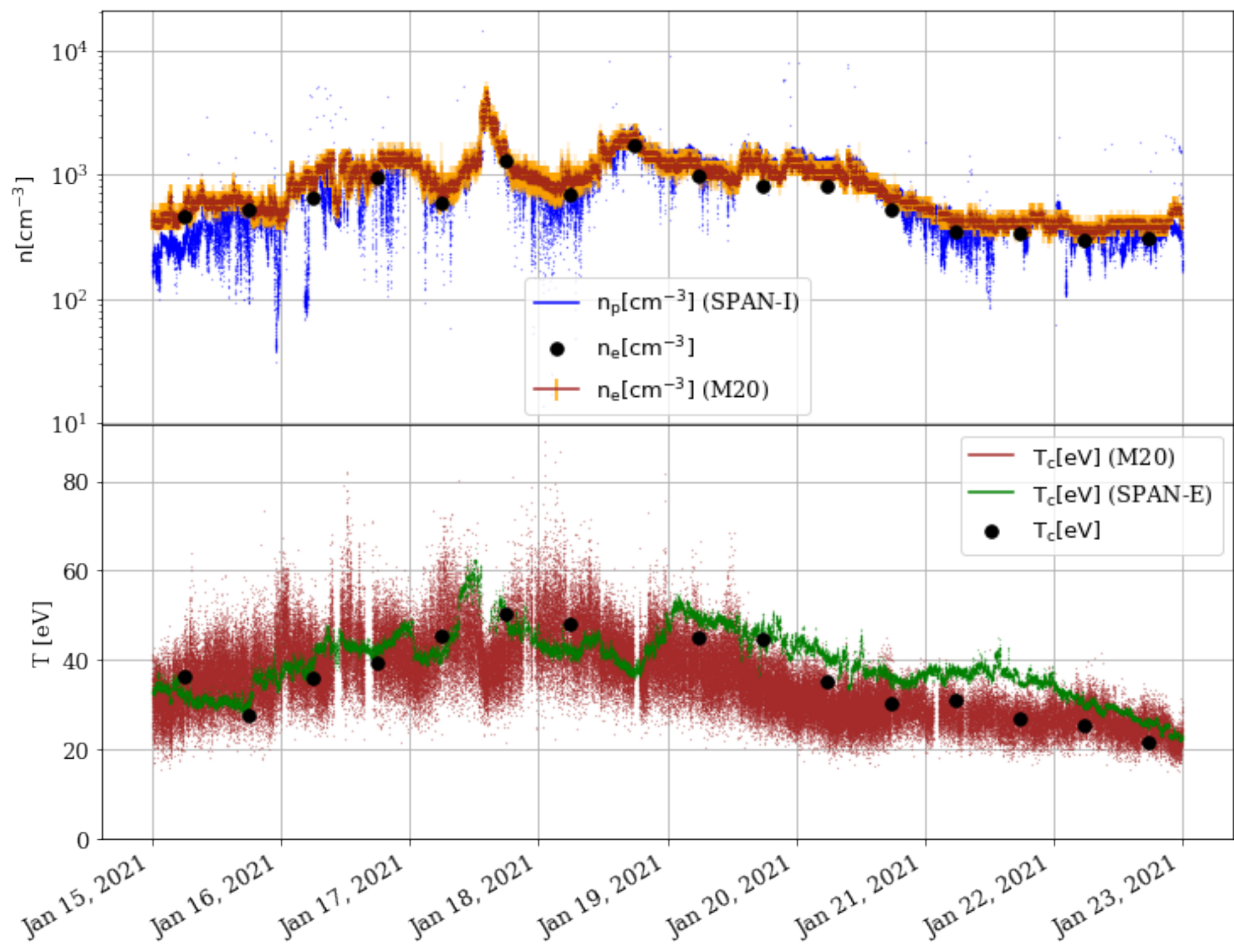


Figure 4.

